

Published in final edited form as:

Magn Reson Med. 2012 October ; 68(4): 1056–1064. doi:10.1002/mrm.24449.

Quantitative chemical exchange sensitive MRI using irradiation with toggling inversion preparation (iTIP)

Tao Jin* and Seong-Gi Kim

Department of Radiology, University of Pittsburgh, Pittsburgh, Pennsylvania, USA

Abstract

Chemical exchange (CE) sensitive MRI contrast acquired with an off-resonance irradiation pulse is affected by other relaxation mechanisms, such as longitudinal and transverse relaxations. In particular, for intermediate chemical exchanges, the effect of transverse relaxation often dominates CE contrast. Since water relaxation rates can change significantly in many pathological conditions or during physiological challenge, it is crucial to separate these relaxation effects in order to obtain pure CE contrast. Here we proposed a novel acquisition scheme in which a toggling inversion pulse is applied prior to the off-resonance irradiation. By combined acquisition of irradiation images with and without an inversion pulse at both the labile proton frequency and the reference frequency, longitudinal and transverse relaxation contributions are cancelled; and the quantification of CE parameters, such as the exchange rate and the labile proton concentration, can be simplified. Furthermore, the CE mediated relaxation rate can be readily determined with a relatively short irradiation pulse and without approaching the steady state, therefore, reducing the limitations on hardware and specific absorption rate requirements. The signal characteristics of the proposed method are evaluated by numerical simulations and phantom experiments.

Keywords

Chemical exchange; spin locking; CEST; toggling inversion preparation; T_1 ; T_2 ; intermediate exchange

Introduction

Chemical exchange (CE) sensitive MRI provides valuable information on tissue pH and metabolite, protein and peptide concentrations; and has been applied to preclinical study of cartilage degeneration, stroke, and tumor (1–9). Previous CE-MRI methods mostly explore labile protons in the slow exchange regime, *i.e.* the exchange rate, k , between water and labile protons is much smaller than their chemical shift, δ ($k/\delta \ll 1$) (1,3,9–13). Recently, there are growing interests in the study of hydroxyl-water exchange (7,14,15) and amine-water exchange (16,17) processes, in which CE is close to the intermediate exchange (IMEX) regime (e.g., $\sim 0.3 < k/\delta < \sim 3$). Compared to slow exchange cases, the IMEX contrast has very different properties and is more difficult to characterize. For example, the specificity of labile protons decrease with increasing k , and the optimal imaging contrast is often achieved at the transient state without a long irradiation pulse (16).

During an off-resonance irradiation pulse, the effective B_1 field in the rotating frame is tilted away from the Z -axis and, thus, the measured water signal is affected by both R_1 and R_2 relaxations (18,19). Specifically, with a relatively high irradiation pulse power (B_1) tuned to

*Corresponding author: Tao Jin, Department of Radiology, University of Pittsburgh, 3025 E Carson Street, Pittsburgh, PA, 15203, taj6@pitt.edu, (Tel) 412-383-8010, (Fax) 412-383-6799.

the IMEX process (16,20), as will be shown later, the CE contrast will be greatly affected by the R_2 relaxation, and also the magnetization transfer (MT) effect due to immobile macromolecules. Since water R_2 and/or R_1 may change significantly in many pathological conditions (2,16,21), it is critical to separate these relaxation effects from pure CE contrast. To simplify the quantification of CE, Sun recently proposed a ratiometric analysis approach that utilizes a long irradiation pulse to obtain steady state signals for purposes of normalization and separating R_1 and R_2 effects (22). One practical issue is that a long irradiation pulse of several seconds is often limited by MR hardware capability and specific absorption rate (SAR) restrictions, especially at high magnetic field strengths and large B_1 power levels needed for IMEX applications. Moreover, in these applications, the steady state signal can be very low and leads to quantification errors using ratiometric normalization.

In this study, we propose a novel acquisition method, dubbed irradiation with toggling inversion preparation (iTIP), to remove the R_1 and R_2 contributions in CE sensitive imaging, and to simplify the quantification of CE parameters. Numerical simulations and phantom experiments were performed to examine the signal characteristics and to validate our theoretical predictions.

Theory

Optimized irradiation time versus the steady state signal

When the populations of two exchangeable proton pools are highly unequal, *i. e.* $p_A \gg p_B$, where p_A and p_B are the relative populations of water and labile solute protons ($p_A + p_B = 1$), respectively, the relaxation rate $R_{1\rho}$ can be expressed as (23):

$$R_{1\rho} = R_1 \cos^2 \theta + (R_2 + R_{ex}) \sin^2 \theta, \quad [1]$$

where $\theta = \arctan(\omega_1/\Omega)$, Ω is the frequency offset from water and ω_1 is the Rabi frequency ($= \gamma \cdot B_1$) of the irradiation pulse. The exchange-mediated relaxation rate is

$$R_{ex} = \frac{p_A \cdot p_B \cdot \delta^2 \cdot k}{(\delta - \Omega)^2 + \omega_1^2 + k^2} \approx \frac{p_B \cdot \delta^2 \cdot k}{(\delta - \Omega)^2 + \omega_1^2 + k^2}, \quad [2]$$

assuming $p_A \approx 1$ and $R_2 - R_1 \ll k$.

Fig. 1A shows the pulse sequence for the proposed iTIP approach, where a toggling inversion pulse is applied preceding an off-resonance spin-locking (SL) module. When the inversion pulse is toggled “off”, the 1st radiofrequency (RF) pulse in an ideal SL experiment

flips the water magnetization by an angle θ to the $B_{1,eff}$ ($= 2\pi \sqrt{\Omega^2 + \omega_1^2} / \gamma$) direction, such that it will be “locked” during the subsequent irradiation pulse and will decay with the relaxation rate $R_{1\rho}$ (Fig. 1B). In practice, the flip angle may not be accurate and is assumed to be a different angle, φ , here. Thus, the magnetization precesses around $B_{1,eff}$ with an angle $\theta - \varphi$ (Fig. 1B), and the chemical exchange saturation transfer (CEST) acquisition scheme corresponds to the case of $\varphi = 0$ (24). In most circumstances, the component perpendicular to the $B_{1,eff}$ direction dephases quickly due to inhomogeneities in B_1 and B_0 and can be ignored. After the spin-locking pulse with duration of TSL , the magnetization parallel to the $B_{1,eff}$ direction (red arrow) is flipped back by the 2nd φ -pulse for imaging (Fig. 1C). The normalized magnetization can be expressed as (16):

$$M_{SL}(\Omega) \equiv S(\Omega)/S_0 = C^2 \cdot e^{-R_{1\rho} \cdot TSL} + S_{SS} \cdot C \cdot (1 - e^{-R_{1\rho} \cdot TSL}) \quad [3]$$

where the normalized steady state signal is $S_{SS} = R_1 \cdot \cos\theta / R_{1\rho}$, $C = \cos(\theta - \varphi)$ equals 1 for ideal SL and $\cos\theta$ for CEST. The TSL value for optimized CE contrast can be derived from Eq. [3]. Assuming $C = 1$, we have (16)

$$TSL_{optimal}(\omega_1) = \frac{1}{R_{1\rho} - R_1 \cos\theta} = \frac{T_{1\rho}}{(1 - S_{SS})} \quad [4]$$

Note that the $T_{1\rho}$ value is always between T_1 and T_2 (Eq. [1]). Thus, the CE contrast will be maximized at a long TSL if S_{SS} is high, *i.e.* a high steady state (HSS) condition, which is mostly seen with very small θ as in slow exchange applications, and at a short TSL if $S_{SS} \ll 1$, *i.e.* a low steady state (LSS) condition, which often occurs for IMEX applications.

Magnetization and asymmetric analysis for the iTIP approach

In Eq. [3], $M_{SL}(\Omega)$ is dependent on R_1 , R_2 , R_{ex} as well as ω_1 and TSL , and it is difficult to separate R_{ex} from R_1 and R_2 . In the iTIP approach, when the inversion pulse is toggled “on”, the water magnetization will still be “locked” by the $B_{1,eff}$, and will recover from the negative magnetization by the same $R_{1\rho}$ to the same steady state (Fig. 1D). The normalized magnetization can be expressed as:

$$M_{iSL}(\Omega) = -\alpha \cdot C^2 \cdot e^{-R_{1\rho} \cdot TSL} + S_{SS} \cdot C \cdot (1 - e^{-R_{1\rho} \cdot TSL}), \quad [5]$$

where α is the inversion efficiency that equals 1 for ideal inversion. The difference between the “on” and “off” preparation yields:

$$M_{iTIP}(\Omega) \equiv \frac{[M_{SL}(\Omega) - M_{iSL}(\Omega)]}{2} = \frac{(1 + \alpha)}{2} \cdot C^2 \cdot e^{-R_{1\rho} \cdot TSL} \quad [6]$$

The difference is halved in Eq. [6] for sensitivity comparison with M_{SL} , because the number of acquired images is doubled in M_{iTIP} . The CE contrast is often assessed from the difference between M_{SL} measured at the labile proton frequency δ (label frequency) and at the reference frequency of $-\delta$, which is referred to as the asymmetry analysis (20):

$$SLR_{asym}(\Omega = \delta) \equiv M_{SL}(-\delta) - M_{SL}(\delta) \quad [7]$$

Similarly, we have

$$SLR_{iTIP,asym}(\Omega = \delta) \equiv M_{iTIP}(-\delta) - M_{iTIP}(\delta) \quad [8]$$

Beside the widely used absolute asymmetry defined by Eq. [7] (similar to MTR_{asym} , the magnetization transfer ratio asymmetry of CEST applications), several studies have adopted a relative asymmetry, where the differential signal is normalized by the signal at the reference frequency instead of S_0 (7,17,24,25):

$$Rel_{asym}(\Omega = \delta) \equiv \frac{M_{SL}(-\delta) - M_{SL}(\delta)}{M_{SL}(-\delta)} \quad [9]$$

Quantification of the exchange-mediated relaxation rate

$R_{1\rho}$ can be obtained by a mono-exponential fitting of TSL in iTIP data using Eq. [6], or by fitting of regular SL data using Eq. [3]. To remove the R_1 and R_2 contribution, we subtract the $R_{1\rho}$ of the reference frequency ($-\Omega$) from the $R_{1\rho}$ at a frequency offset of Ω :

$$\begin{aligned} R_{1\rho,asym}(\Omega) &\equiv R_{1\rho}(\Omega) - R_{1\rho}(-\Omega) = \frac{1}{TSL} \cdot \ln \frac{M_{iTIP}(-\Omega)}{M_{iTIP}(\Omega)} \\ &= [R_{ex}(\Omega) - R_{ex}(-\Omega)] \cdot \frac{\omega^2}{\omega^2 + \Omega^2} \end{aligned} \quad [10]$$

From Eq. [10], the major advantage of the iTIP approach over the conventional SL approach is that $R_{1\rho,asym}$ can be obtained from iTIP data with a single TSL measurement. When $\Omega = \delta$,

$$R_{1\rho,asym}(\Omega=\delta) = p_B k \cdot \frac{1}{1 + \frac{k^2}{\omega_1^2}} \cdot \frac{1}{1 + \frac{\omega_1^2}{\delta^2}} \cdot \frac{1}{1 + \frac{\omega_1^2 + k^2}{4\delta^2}} \quad [11]$$

which is only dependent on the exchange parameters p_B and k and does not have R_1 and R_2 relaxation terms, and is also independent of the inversion efficiency α and the flip angle φ .

Materials and Methods

Numerical Simulations

Numerical simulations were performed in Matlab[®] 7.0 using Bloch-McConnell Equations. A three-compartment exchange was simulated, where the water pool exchanges with a labile solute proton pool and an immobile proton pool, and the relative population for each compartment is P_w , P_S , and P_{im} ($P_w + P_S + P_{im} = 1$), respectively. Note that in the theory section only water and solute proton populations were considered, thus the relative population can be converted as $p_A = P_w/(P_w + P_S)$, and $p_B = P_S/(P_w + P_S)$. The MT effect between water and bound protons associated with immobile macromolecules was modeled as a super-Lorentzian function (26,27), and incorporated into the Bloch-McConnell Equations following the work of Li et al (10). Without loss of generality, we assumed a chemical shift between water and the labile protons of $\delta = 1$ ppm (400 Hz or 2515 rad·s⁻¹ at 9.4 T), an exchange rate of $k = 1250$ s⁻¹ (*i.e.*, $k/\delta = 0.5$), and $C = \alpha = 1$. Two irradiation pulse powers were chosen in the simulation to compare signal properties with HSS and LSS conditions. An HSS condition will be reached with $\omega_1 = 40$ Hz and $R_2 = 1$ s⁻¹, and an LSS condition with $\omega_1 = 160$ Hz and $R_2 = 15$ s⁻¹. To examine the signal characteristics of iTIP as a function of TSL , the M_{SL} , M_{iSL} , M_{iTIP} , SLR_{asym} , $SLR_{iTIP,asym}$, and Rel_{asym} were calculated for $\omega_1 = 160$ Hz (1000 rad·s⁻¹). Due to the B_1 -tuning effect, this pulse power would be most sensitive to CE rate around 1000 s⁻¹ (16). At each TSL , $R_{1\rho}$ and $R_{1\rho,asym}$ were calculated using Eq. [6] and [10], respectively. As a qualitative example, the $R_{1\rho}$ and $R_{1\rho,asym}$ dispersions with an ω_1 range of 10 to 800 Hz were also simulated for quantification of exchange parameters. All other parameters used in the simulation were listed in Table 1.

MR experiments

All MR experiments were performed at room temperature on a 9.4 T Varian system. A 3.8-cm diameter volume coil (Rapid Biomedical, Ohio, USA) was used for excitation and reception. Magnetic field homogeneity was optimized by localized shimming over the volume of interest to yield a water spectral linewidth within 9–15 Hz. B_1 fields were mapped for calibration of the transmit power (28), B_0 maps were measured by gradient-echo

echo-planar imaging (EPI) with multiple echo times, R_1 maps were measured by an inversion recovery sequence, and R_2 maps were measured by an on-resonance spin-locking sequence with $\omega_1 = 4000$ Hz to suppress the chemical exchange contributions (16). MR images were acquired using the iTIP scheme (Fig. 1A). After the preparation pulses, images were collected by single-shot spin-echo EPI with a field of view of $40 \text{ mm} \times 40 \text{ mm}$, a slice thickness of 5 mm, matrix size of 64×64 , and a post-imaging recovery time of 15 s. Control scans were acquired at $\Omega = 300$ ppm for normalization of M_{SL} .

Three types of metabolite phantoms were imaged. Metabolite solutions were prepared and transferred into 9 mm I.D. cylinders and multiple cylinders were bundled together for iTIP imaging studies. To obtain M_{iTIP} maps, SL images with inversion preparation “off” and “on” were acquired sequentially. Three SL imaging studies were:

1. 50 mM myo-Inositol (Ins, cyclohexane-1,2,3,4,5,6-hexol, $\text{C}_6\text{H}_{12}\text{O}_6$) was dissolved in phosphate buffered saline (PBS) (pH = 7.4), and 0.025, 0.05, 0.075, and 0.1 mM MnCl_2 was added to modulate both R_1 and R_2 . Ins has hydroxyl protons with a chemical shift of ~ 0.93 ppm from water and an exchange rate of about 1250 s^{-1} , thus $k/\delta \approx 0.53$ and is in the IMEX regime (29). The iTIP images at $\Omega = 0.95$ and -0.95 ppm were acquired with $\omega_1 = 100$ Hz and 160 Hz, and TSL values from 0 to 4 s.
2. To modulate water R_2 and also introduce the magnetization transfer effect, 50 mM Ins was dissolved in PBS (pH = 7.4), and mixed in 0.5, 1, 2 and 3% agar. The mixtures were heated to $90\text{--}95^\circ\text{C}$ in a water bath for 2–3 minutes, cooled down to 60°C and transferred to plastic cylinders to solidify. The iTIP images at $\Omega = 0.95$ and -0.95 ppm were acquired with $\omega_1 = 100$ Hz and 160 Hz, and TSL values from 0 to 1.5 s.
3. 50 mM Creatine (Cr, 2-(Methylguanidino)ethanoic acid, $\text{C}_4\text{H}_9\text{N}_3\text{O}_2$) was dissolved in PBS and titrated to pH = 7.4, 7.7, 8.05, and 8.4. Cr has exchangeable guanidine protons (i.e., $\text{NH}_2 - \text{C}(\text{NH}_2)_2$) at 1.9 ppm from the water resonance (30). These pH values were selected so that the exchange will be close to the IMEX regime. At lower pH values, the exchange between water and Cr guanidine protons is in the slow exchange domain, and has been thoroughly studied by Sun et al. using CEST models (22,31,32). The iTIP images were acquired at $\Omega = 1.9$ and -1.9 ppm. Off-resonance $R_{1\rho}$ dispersion was measured using twelve ω_1 values of approximately 85, 107, 135, 170, 214, 270, 340, 428, 540, 680, 857, and 1080 Hz. For each power level, iTIP images were acquired with twelve TSL values. Because $R_{1\rho}$ increases with ω_1 , the range of TSL varied accordingly, e. g. from 0 to 3 s for small ω_1 of 85 Hz and from 0 to 0.4 s for 1080 Hz. In addition, on-resonance $R_{1\rho}$ dispersion was measured using ω_1 value of approximately 125, 177, 250, 353, 500, 707, 1000, 1414, 2000, 2828, and 4000 Hz.

Data analysis

To obtain M_{iTIP} , pair-wise subtraction between SL images with inversion pulse “on” and “off” were performed in k -space before the image reconstruction. $R_{1\rho}$ maps were calculated from fitting of multi- TSL data to Eq. [6], and $R_{1\rho, \text{asym}}$ maps were calculated from M_{iTIP} maps at each TSL using Eq. [10]. For quantitative analysis, a region of interest (ROI) with minimal B_0 heterogeneity (< 3 Hz) was selected from each sample. The $R_{1\rho, \text{asym}}$ dispersion data were fitted to Eq. [11] to determine the chemical exchange parameters p_B and k . To fit the on-resonance $R_{1\rho}$ dispersion data, Eqs. [1] and [2] were used with $\theta = 90^\circ$.

Results

M_{SL} versus M_{iTIP}

Fig. 2 shows the simulated iTIP signals for the HSS case (small ω_1 and R_2), and for the LSS case (large ω_1 and R_2). The HSS case (Fig. 2A–C) requires long irradiation of more than 5 s to approach the steady state for both the label (Fig. 2A, black) and reference frequencies (red), where the steady states are the same for SL with the inversion pulse “off” (solid lines) and “on” (dashed lines). In the LSS case (Fig. 2D–F), MR signals decay quickly with TSL and reaching the steady state much faster than the HSS case because of larger $R_{1\rho}$ values (Fig. 2D). In both HSS and LSS cases, M_{iTIP} signals (shown in logarithms scale, Fig. 2B and 2E) are monoexponential functions of TSL , from which $R_{1\rho}$ can be easily calculated. In the HSS condition (Fig. 2C), SLR_{asym} is maximized at TSL approaching the steady state, whereas $SLR_{iTIP, asym}$ peaks at a shorter TSL and is much smaller than SLR_{asym} . In the LSS condition (Fig. 2F), the peaks of both SLR_{asym} and $SLR_{iTIP, asym}$ are reached at short TSL values of ~ 0.35 s. $SLR_{iTIP, asym}$ is still less than SLR_{asym} , but their difference is small.

To compare simulation and experimental results, iTIP data of 50 mM Ins were obtained in 0.05 mM $MnCl_2$ (Fig. 3A–C) and in 2% agar (Fig. 3D–F). The former sample has smaller R_2 and no MT effect. Thus, the steady state signals for $\omega_1 = 100$ Hz are relatively high and require a long irradiation pulse (Fig. 3A). The M_{iTIP} values decay monoexponentially with TSL , except for a few long TSL values with $\Omega = \delta$ in which M_{iTIP} becomes very low and is dominated by noise (Fig. 3B). $SLR_{iTIP, asym}$ is significantly smaller than SLR_{asym} (Fig. 3C), similar to the simulation results of the HSS condition in Fig. 2C. For the Ins in agar phantoms, the steady state signals for $\omega_1 = 160$ Hz are very small due to large R_2 and MT effects (Fig. 3D). The imaging contrast is maximized with a short irradiation pulse for both $SLR_{iTIP, asym}$ and SLR_{asym} , and the peak $SLR_{iTIP, asym}$ is only slightly smaller ($\sim 15\%$) than that of SLR_{asym} (Fig. 3F), similar to the simulation results of the LSS condition in Fig. 2F.

$R_{1\rho, asym}$ is independent of R_1 and R_2

Computer simulations were performed to determine the effect of R_1 , R_2 , and P_{im} on CE contrast indices, for an $\omega_1 = 160$ Hz pulse. SLR_{asym} , $SLR_{iTIP, asym}$ and Rel_{asym} are all sensitive to R_1 , R_2 and P_{im} except for short TSL values (Fig. 4A–4C). Specifically, in both SLR_{asym} and $SLR_{iTIP, asym}$, the optimal TSL values decrease significantly with increasing R_2 and P_{im} . The relative asymmetry (Fig. 4C) minimizes the dependence on R_1 , R_2 and P_{im} for $TSL < \sim 0.3$ s, which is wider than the range for absolute asymmetry ($TSL < 0.1$ s, Fig. 4A), but not for larger TSL values. In contrast, $R_{1\rho, asym}$ is not dependent on R_1 , R_2 and TSL (Fig. 4D). Note that $R_{1\rho, asym}$ was determined at every TSL value with Eq. [10]. The $R_{1\rho, asym}$ for $P_{im} = 0.05$ is about 5% larger than that for $P_{im} = 0$, because for a two-site exchange in Eq. [2], $p_B = P_S/(P_w+P_S) = P_S/(1-P_{im})$ increases with P_{im} .

To experimentally demonstrate the insensitiveness of R_1 and R_2 to $R_{1\rho, asym}$, the R_1 , R_2 , SLR_{asym} , Rel_{asym} , and $R_{1\rho, asym}$ maps were obtained from 50 mM Ins in four different concentrations of $MnCl_2$ (upper row, Fig. 5) and agar (bottom row, Fig. 5). Both R_1 and R_2 increase with the $MnCl_2$ concentration, whereas R_2 and P_{im} increase with agar concentrations. For a short TSL of 0.25 s, the CE contrasts measured with SLR_{asym} and Rel_{asym} are relatively insensitive to changes in R_1 , R_2 and P_{im} . At a longer TSL of 1.0 s, both SLR_{asym} and Rel_{asym} are dependent on R_1 , R_2 as well as P_{im} , and are inversely correlated with R_2 and P_{im} . In contrast, for both TSL values, the dependence on R_1 and R_2 is removed in the $R_{1\rho, asym}$ maps acquired using the iTIP approach. Whereas a small P_{im} dependence is expected for $R_{1\rho, asym}$ from simulation, no significant contrast was observed among the samples, suggesting that the difference of P_{im} may be too small to be detectable

in these agar samples. The insensitiveness of $R_{1\rho, \text{asym}}$ on agar concentration also suggests that the exchange rate is not affected by the addition of MT effect in these phantoms.

Quantification of exchange parameters using $R_{1\rho, \text{asym}}$ dispersion

Exchange parameters p_B and k can be determined from $R_{1\rho, \text{asym}}$ dispersion ($R_{1\rho, \text{asym}}(\Omega = \delta)$ vs. ω_1 plot) with Eq. [11]. The simulated off-resonance $R_{1\rho}$ dispersion increases with R_2 and P_{im} at both the label (Fig. 6A, black) and reference frequencies (red). However, the $R_{1\rho, \text{asym}}$ eliminates these dependences and gives a dispersion which is only related to exchange parameters p_B and k (Fig. 6B).

This approach is experimentally tested. The $R_{1\rho}$ dispersions of Cr phantoms with four pH values were measured by the iTIP approach at both $\Omega = 1.9$ and -1.9 ppm (Fig. 7A and 7B). $R_{1\rho, \text{asym}}$ was calculated from $R_{1\rho}$ of label and reference frequencies (Fig. 7C). The control PBS phantom has the same $R_{1\rho}$ value for 1.9 and -1.9 ppm and was cancelled in the $R_{1\rho, \text{asym}}$, as expected. The exchange rate and labile proton population were obtained by fitting the $R_{1\rho, \text{asym}}$ dispersions (Eq. [11]). For comparison, the on-resonance $R_{1\rho}$ dispersions of these phantoms were obtained in order to calculate the exchange parameters (Fig. 7D). The two fitting procedures of $R_{1\rho, \text{asym}}$ and on-resonance $R_{1\rho}$ dispersions give similar results of the exchange rate, which increases with pH as expected for a base-catalyzed amine-water proton exchange (Fig. 7E). For on-resonance SL, p_B and k cannot be determined separately in the slow exchange regime (20), which is the case for the pH = 7.4 and 7.7 phantoms, so their p_B values were set to be same as the pH = 8.05 sample (indicated by the stars in Fig. 7F). The fitted p_B slightly increases with pH in the $R_{1\rho, \text{asym}}$ results and also in the on-resonance $R_{1\rho}$ dispersion of pH = 8.05 to 8.4. This may be due to the different exchange rates of ηNH_2 and ϵNH protons in Cr (33), leading to small errors in our calculations that assumed a single rate constant.

Discussion

The absolute asymmetry signal (SLR_{asym} or MTR_{asym}) has been widely used as a convenient indicator of CE contrast in the slow exchange regime. In the IMEX regime, however, SLR_{asym} is much more sensitive to other relaxation effects, thus it is no longer a good index for quantitative CE imaging. For instance, the SLR_{asym} obtained for an R_2 and MT effect similar to *in vivo* conditions can be more than 10 times smaller than that of an aqueous solution (cyan versus black curves for $TSL > 0.8$ s, Fig. 4a), and the optimal TSL that maximizes SLR_{asym} is much shorter for the former than the latter. Therefore, care should be exercised when comparing SLR_{asym} or MTR_{asym} measured under different conditions. In a previous study of IMEX metabolites including glutamate and glucose, we reported that the frequency offset of the SLR_{asym} peak shifts with pH as well as with labile proton concentrations (29). Although the relative asymmetry, as defined in Eq. [9], can alleviate some of these problems at short TSL values, our results of current and previous studies show that the asymmetry of exchange-mediate relaxation rate ($R_{1\rho, \text{asym}}$ or $R_{\text{ex, asym}}$) would be most suitable for quantitative CE imaging in the IMEX regime.

Our proposed iTIP approach can simplify quantitative CE imaging in two ways. (1) Multi- TSL measurements with long TSL values approaching the steady state are necessary for accurate fitting of $R_{1\rho}$ using Eq. [3] (or Eq. [5]). Using iTIP, M_{iTIP} is a mono-exponential function of $R_{1\rho}$ that reduces the fitting parameters, so that $R_{1\rho}$ can be determined more accurately and with shorter TSL . (2) The CE contrast acquired by an off-resonance irradiation is affected by R_1 and R_2 . These relaxation effects are canceled out in $R_{1\rho, \text{asym}}$, which simplify the quantification of exchange parameters. In fact, $R_{1\rho, \text{asym}}$ can be readily obtained from iTIP data at a single TSL value, and also without the necessity to acquire a control scan (300 ppm in this study) for normalization. This is clearly advantageous over

conventional off-resonance irradiation approaches that require multiple TSL values because data acquisition time is greatly shortened.

Technically, the iTIP quantification of $R_{1\rho}$ is independent of the flip angle in the SL preparation (Eq. [6]), and thus can be acquired with the conventional CEST scheme. It is also insensitive to inversion efficiency and theoretically can be acquired with a toggling saturation pulse or any two pulses with different initial magnetizations. While our simulation and phantom experiments mainly targeted IMEX process, the iTIP approach can also be applied to slow exchange applications. Because the iTIP contrast is greatly reduced at a long irradiation time (Fig. 2C and 3C), it would be best suitable for IMEX studies where the contrast is optimized at the transient state, or for slow exchange studies where a long irradiation pulse is unavailable because of hardware or SAR limitations.

Off-resonance irradiation with a preceding inversion preparation has been suggested or applied in MT and CEST studies (24,34–37). In MRI, Mangia et al. showed that the combination of MT-weighted images acquired with and without inversion preparation improves the quantification accuracy of MT rate (36). Vinogradov et al. applied an inversion pulse before irradiation of labile protons to obtain positive CEST imaging contrast, which was smaller in magnitude than conventional CEST that gives negative contrast (37). Indeed, our simulation and experimental results also showed that the CE contrast is reduced with the inversion preparation “on” for the HSS condition (Fig 2A and 3A), but the loss of iTIP contrast becomes very small for LSS cases.

Although both on-resonance $R_{1\rho}$ and $R_{1\rho, \text{asym}}$ are sensitive to the IMEX process, $R_{1\rho, \text{asym}}$ can also be tuned to slow chemical exchange using low B_1 , unlike on-resonance $R_{1\rho}$ (20). On the other hand, the asymmetry analysis of $R_{1\rho, \text{asym}}$ greatly reduces the sensitivity when the exchange rate is near the fast exchange regime ($k \gg \delta$, see Eq. [11]), for which on-resonance $R_{1\rho}$ may be more sensitive. Besides this difference in sensitivity regimes, iTIP quantification of IMEX using $R_{1\rho, \text{asym}}$ dispersion has a few advantages. For example, (1) $R_{1\rho, \text{asym}}$ can be acquired selectively for a specific type or a certain group of labile protons in contrast to on-resonance $R_{1\rho}$, which has contributions from all relaxation pathways. (2) A lower ω_1 is necessary for quantification of exchange parameters because off-resonance irradiation increases the effective B_1 (see Fig. 7), which alleviates the burden on hardware and SAR limitations. (3) $R_{1\rho, \text{asym}}$ dispersion (Eq. [11]) cancels the R_2 term and, therefore, has fewer fitting parameters. (4) As mentioned earlier, $R_{1\rho, \text{asym}}$ can be obtained with a single TSL for each ω_1 value and, therefore, reduces the acquisition time.

Only one labile proton pool is considered in this proof-of-principle study. *In vivo* there are many different IMEX protons, and some of them are similar in frequency offset. Since the specificity of labile protons are inversely dependent on the linewidth of $R_{\text{ex}} (= \sqrt{\omega_1^2 + k^2}$, from Eq. [2]), it would be very difficult to distinguish two populations of labile protons if the linewidths of R_{ex} for both species are comparable or larger than the chemical shifts between them. Due to this intrinsic limitation of off-resonance irradiation approaches, the *in vivo* quantification of IMEX may only be achieved for a group-average of labile protons with similar chemical shifts and exchange rates, *e. g.* amine- or hydroxyl-groups.

Similar to the problems encountered in CEST studies, *in vivo* quantification using $R_{1\rho, \text{asym}}$ is also susceptible to B_0 and B_1 inhomogeneities as well as the intrinsic asymmetry of the MT effect from immobile macromolecules (38). Both variations in B_0 and B_1 will lead to error in the exchange-mediate relaxation rate (Eq. [1] and [2]), and the former will also cause error in the calculation of $R_{1\rho, \text{asym}}$ and incomplete cancelation of R_1 and R_2 . To alleviate the inhomogeneous B_0 problem, iTIP images may be acquired at multiple offsets around the label and reference frequencies for B_0 correction if a severe B_0 shift is present.

Similarly, a B_1 calibration procedure may be performed to correct the $R_{1\rho, \text{asym}}$ quantification error caused by B_1 inhomogeneity (39). Further simulations and modeling studies are necessary to evaluate the effect of MT asymmetry on $R_{1\rho, \text{asym}}$ and its dispersion, and whether it can be minimized by adjusting irradiation parameters.

Conclusions

In the IMEX regime, CE contrast is greatly affected by other relaxation effects. With the proposed iTIP approach, $R_{1\rho, \text{asym}}$ (or similarly, $R_{\text{ex, asym}}$), which removes the R_1 and R_2 relaxation effects, is readily determined, and the quantification of chemical exchange parameters can be simplified. In addition, the iTIP approach is insensitive to inversion efficiency and flip angle for SL, and does not rely on long irradiation pulses. Therefore, this novel acquisition method can be very useful for slow to intermediate exchange or high-field CE applications.

Acknowledgments

We thank Kristy Hendrich for maintaining the 9.4 T system, and Dr. Alex Poplawsky for proofreading. This work is supported by NIH grants EB008717, EB003324, EB003375, and NS44589.

References

1. Zhou JY, Payen JF, Wilson DA, Traystman RJ, van Zijl PCM. Using the amide proton signals of intracellular proteins and peptides to detect pH effects in MRI. *Nat Med.* 2003; 9(8):1085–1090. [PubMed: 12872167]
2. Zhou JY, Tryggstad E, Wen ZB, Lal B, Zhou TT, Grossman R, Wang SL, Yan K, Fu DX, Ford E, Tyler B, Blakeley J, Larterra J, van Zijl PCM. Differentiation between glioma and radiation necrosis using molecular magnetic resonance imaging of endogenous proteins and peptides. *Nat Med.* 2011; 17(1):130–U308. [PubMed: 21170048]
3. Sun PZ, Zhou JY, Sun WY, Huang J, van Zijl PCM. Detection of the ischemic penumbra using pH-weighted MRI. *Journal of Cerebral Blood Flow and Metabolism.* 2007; 27(6):1129–1136. [PubMed: 17133226]
4. Jia GA, Abaza R, Williams JD, Zynger DL, Zhou JY, Shah ZK, Patel M, Sammet S, Wei L, Bahnson RR, Knopp MV. Amide Proton Transfer MR Imaging of Prostate Cancer: A Preliminary Study. *Journal of Magnetic Resonance Imaging.* 2011; 33(3):647–654. [PubMed: 21563248]
5. Grohn OHJ, Lukkarinen JA, Silvennoinen MJ, Pitkanen A, van Zijl PCM, Kauppinen RA. Quantitative magnetic resonance imaging assessment of cerebral ischemia in rat using on-resonance T-1 in the rotating frame. *Magnetic Resonance in Medicine.* 1999; 42(2):268–276. [PubMed: 10440951]
6. Jokivarsi KT, Hiltunen Y, Grohn H, Tuunanen P, Grohn OHJ, Kauppinen RA. Estimation of the Onset Time of Cerebral Ischemia Using T-1 rho and T-2 MRI in Rats. *Stroke.* 2010; 41(10):2335–2340. [PubMed: 20814006]
7. Ling W, Regatte RR, Navon G, Jerschow A. Assessment of glycosaminoglycan concentration in vivo by chemical exchange-dependent saturation transfer (gagCEST). *Proceedings of the National Academy of Sciences of the United States of America.* 2008; 105(7):2266–2270. [PubMed: 18268341]
8. Schmitt B, Zbyn S, Stelzeneder D, Jellus V, Paul D, Lauer L, Bachert P, Trattnig S. Cartilage quality assessment by using glycosaminoglycan chemical exchange saturation transfer and (23)Na MR imaging at 7 T. *Radiology.* 2011; 260(1):257–264. [PubMed: 21460030]
9. Jokivarsi KT, Grohn HI, Grohn OH, Kauppinen RA. Proton transfer ratio, lactate, and intracellular pH in acute cerebral ischemia. *Magnetic Resonance in Medicine.* 2007; 57(4):647–653. [PubMed: 17390356]
10. Li AX, Hudson RHE, Barrett JW, Jones CK, Pasternak SH, Bartha R. Four-Pool Modeling of Proton Exchange Processes in Biological Systems in the Presence of MRI-Paramagnetic Chemical

- Exchange Saturation Transfer (PARACEST) Agents. *Magnetic Resonance in Medicine*. 2008; 60(5):1197–1206. [PubMed: 18958857]
11. Woessner DE, Zhang SR, Merritt ME, Sherry AD. Numerical solution of the Bloch equations provides insights into the optimum design of PARACEST agents for MRI. *Magnetic Resonance in Medicine*. 2005; 53(4):790–799. [PubMed: 15799055]
 12. Dixon WT, Ren JM, Lubag AJM, Ratnakar J, Vinogradov E, Hancu I, Lenkinski RE, Sherry AD. A Concentration-Independent Method to Measure Exchange Rates in PARACEST Agents. *Magnetic Resonance in Medicine*. 2010; 63(3):625–632. [PubMed: 20187174]
 13. Jin, T.; Wang, P.; Zong, X.; Kim, SG. *Magn Reson Med* 2012(MR imaging of the amide-proton transfer effect and the pH-insensitive nuclear Overhauser effect at 9.4 T). In press
 14. van Zijl PCM, Jones CK, Ren J, Malloy CR, Sherry AD. MRI detection of glycogen in vivo by using chemical exchange saturation transfer imaging (glycoCEST). *Proceedings of the National Academy of Sciences of the United States of America*. 2007; 104(11):4359–4364. [PubMed: 17360529]
 15. Haris M, Cai K, Singh A, Hariharan H, Reddy R. in vivo mapping of brain myo-inositol. *Neuroimag*. 2011; 54:2079–2085.
 16. Jin T, Wang P, Zong X, Kim SG. Magnetic resonance imaging of the Amine-Proton EXchange (APEX) dependent contrast. *Neuroimag*. 2012; 59:1218–1227.
 17. Cai K, Haris M, Singh A, Kogan F, Greenburg ME, Haris M, Detre J, Reddy R. Magnetic resonance imaging of glutamate. *Nature Med*. 2012; 18(2):302–306. [PubMed: 22270722]
 18. Santyr GE, Fairbanks EJ, Kelcz F, Sorenson JA. Off-Resonance Spin Locking for Mr-Imaging. *Magnetic Resonance in Medicine*. 1994; 32(1):43–51. [PubMed: 8084236]
 19. Grohn OHJ, Makela HI, Lukkarinen JA, DelaBarre L, Lin J, Garwood M, Kauppinen RA. On- and off-resonance T-1 rho MRI in acute cerebral ischemia of the rat. *Magnetic Resonance in Medicine*. 2003; 49(1):172–176. [PubMed: 12509834]
 20. Jin T, Autio J, Obata T, Kim SG. Spin-locking versus chemical exchange saturation transfer MRI for investigating chemical exchange process between water and labile metabolite protons. *Magnetic Resonance in Medicine*. 2011; 65(5):1448–1460. [PubMed: 21500270]
 21. Sun PZ, Cheung JS, Wang EF, Lo EH. Association between pH-weighted endogenous amide proton chemical exchange saturation transfer MRI and tissue lactic acidosis during acute ischemic stroke. *Journal of Cerebral Blood Flow and Metabolism*. 2011; 31(8):1743–1750. [PubMed: 21386856]
 22. Sun PZ. Simplified quantification of labile proton concentration-weighted chemical exchange rate ($k(ws)$) with RF saturation time dependent ratiometric analysis (QUESTRA): Normalization of relaxation and RF irradiation spillover effects for improved quantitative chemical exchange saturation transfer (CEST) MRI. *Magn Reson Med*. 2012 in press.
 23. Trott O, Palmer AG. R-1 rho relaxation outside of the fast-exchange limit. *Journal of Magnetic Resonance*. 2002; 154(1):157–160. [PubMed: 11820837]
 24. Ward KM, Aletras AH, Balaban RS. A new class of contrast agents for MRI based on proton chemical exchange dependent saturation transfer (CEST). *Journal of Magnetic Resonance*. 2000; 143(1):79–87. [PubMed: 10698648]
 25. Liu GS, Gilad AA, Bulte JWM, van Zijl PCM, McMahon MT. High-throughput screening of chemical exchange saturation transfer MR contrast agents. *Contrast Media Mol Imaging*. 2010; 5(3):162–170. [PubMed: 20586030]
 26. Morrison C, Stanisiz GJ, Henkelman RM. Modeling magnetization transfer for biological-like systems using a semi-solid pool with super-Lorentzian lineshape and dipolar reservoir. *J Magn Reson B*. 1995; 108:103–113. [PubMed: 7648009]
 27. Morrison C, Henkelman RM. A model for magnetization transfer in tissue. *Magn Reson Med*. 1995; 33:475–482. [PubMed: 7776877]
 28. Jin T, Kim S-G. Change of the cerebrospinal fluid volume during brain activation investigated by T1 ρ -weighted fMRI. *Neuroimag*. 2010; 51(4):1378–1383.
 29. Jin, T.; Kim, SG. Water-metabolite hydroxyl proton exchange studied using spin-locking and chemical exchange saturation transfer approaches. Montreal, Canada. Proc 19th ISMRM Annual Meeting; 2011. p. 708

30. Sun PZ, Farrar CT, Sorensen AG. Correction for artifacts induced by B-0 and B-1 field inhomogeneities in pH-Sensitive chemical exchange saturation transfer (CEST) Imaging. *Magnetic Resonance in Medicine*. 2007; 58(6):1207–1215. [PubMed: 17969015]
31. Sun PZ, Benner T, Kumar A, Sorensen AG. Investigation of optimizing and translating pH-sensitive pulsed-chemical exchange saturation transfer (CEST) imaging to a 3T clinical scanner. *Magnetic Resonance in Medicine*. 2008; 60(4):834–841. [PubMed: 18816867]
32. Sun PZ, Sorensen AG. Imaging pH using the chemical exchange saturation transfer (CEST) MRI: Correction of concomitant RF irradiation effects to quantify CEST MRI for chemical exchange rate and pH. *Magnetic Resonance in Medicine*. 2008; 60(2):390–397. [PubMed: 18666128]
33. Liepinsh E, Otting G. Proton exchange rates from amino acid side chains - Implications for image contrast. *Magnetic Resonance in Medicine*. 1996; 35(1):30–42. [PubMed: 8771020]
34. Akasaka K. Longitudinal Relaxation of Protons under Cross Saturation and Spin Diffusion. *Journal of Magnetic Resonance*. 1981; 45(2):337–343.
35. Akasaka K, Ishima R, Shibata S. Proton Spin Relaxation in Biopolymers at High Magnetic-Fields. *Physica B*. 1990; 164(1–2):163–179.
36. Mangia S, De Martino F, Liimatainen T, Garwood M, Michaeli S. Magnetization transfer using inversion recovery during off-resonance irradiation. *Magnetic Resonance Imaging*. 29(10):1346–1350. [PubMed: 21601405]
37. Vinogradov E, Soesbe TC, Balschi JA, Sherry AD, Lenkinski RE. pCEST: Positive contrast using Chemical Exchange Saturation Transfer. *J Magn Reson*. 2012; 215:64–73. [PubMed: 22237630]
38. Hua J, Jones CK, Blakeley J, Smith SA, van Zijl PCM, Zhou JY. Quantitative description of the asymmetry in magnetization transfer effects around the water resonance in the human brain. *Magnetic Resonance in Medicine*. 2007; 58(4):786–793. [PubMed: 17899597]
39. Singh A, Cai K, Haris M, Hariharan H, Reddy R. On B(1) inhomogeneity correction of in vivo human brain glutamate chemical exchange saturation transfer contrast at 7T. *Magn Reson Med*. 2012.10.1002/mrm.24290

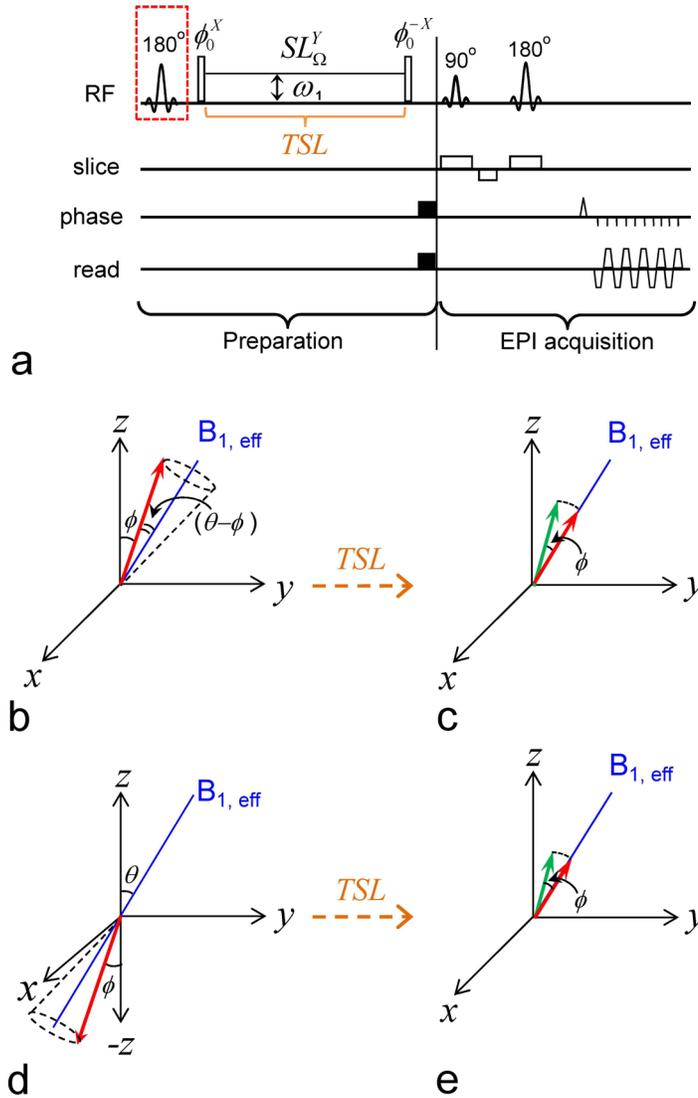


Fig. 1. Pulse sequence and magnetization trajectories

(A) Pulse sequence for the Irradiation with Toggling Inversion Preparation (iTIP) approach. A spin-locking (SL) module is applied following a toggling inversion pulse, indicated by a red dashed square. The super- and subscripts of an RF pulse denotes its phase and transmitter frequency, respectively. Water magnetization differs at the initial condition with inversion pulse toggled “off” (B–C) and “on” (D–E). In either case, the water magnetization is flipped by a ϕ pulse and then “locked” by an SL pulse with frequency offset Ω , a Rabi frequency of ω_1 and a spin-locking time (TSL). Consequently, the water magnetization (red arrow) precesses around $B_{1,eff}$ by an angle $(\theta - \phi)$, relaxes with time constant $R_{1\rho}$ (B, D), and reaches the same steady state if TSL is sufficiently long. For finite TSL in the transient state, the magnetization is larger than the steady state in (C), whereas it is smaller than the steady state in (E). Following the SL pulse, the 2nd ϕ pulse flips the magnetization (red arrow) back toward the Z-axis for imaging (green arrow). The image readout is EPI in this example, but can be replaced by other fast acquisition methods.

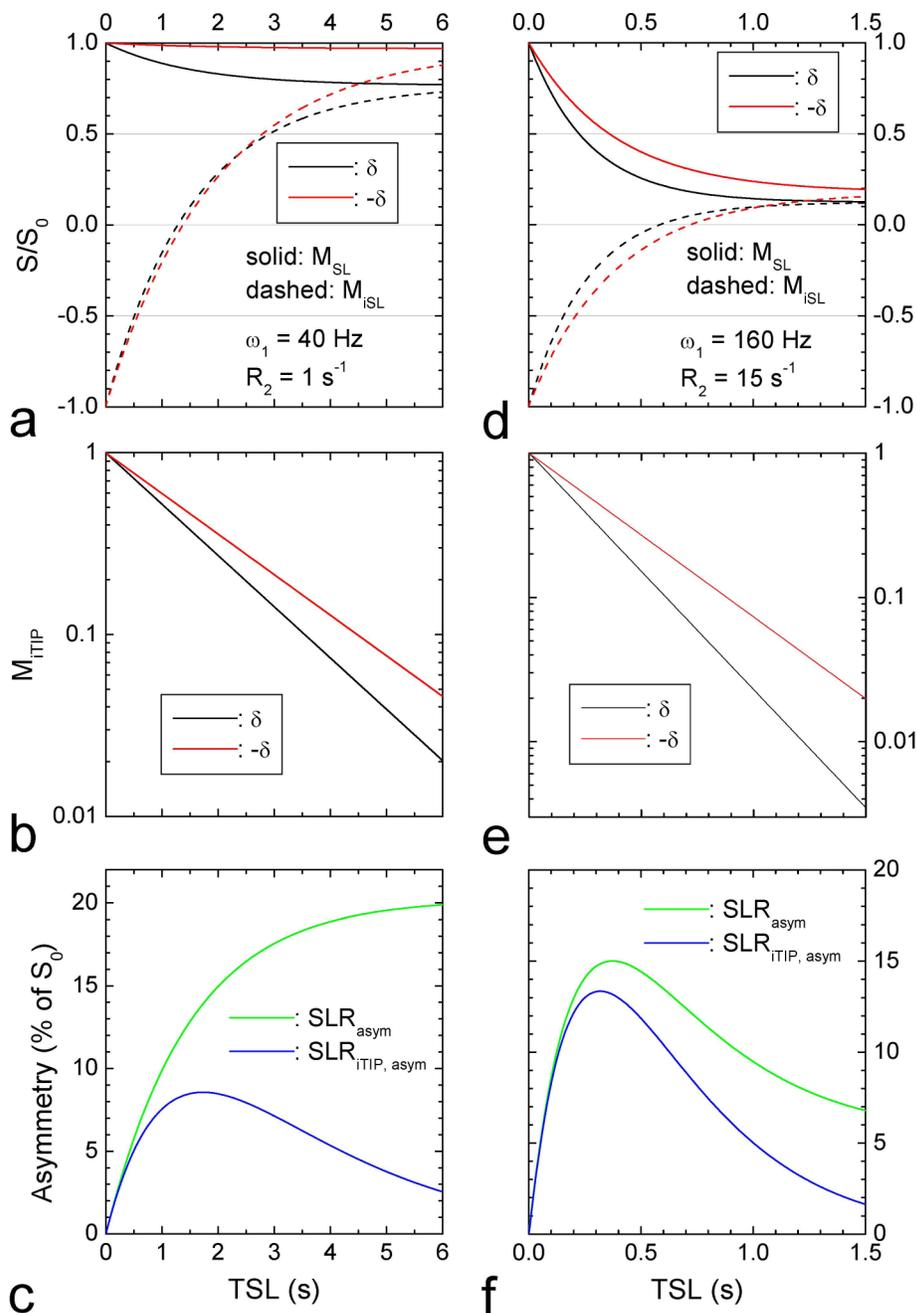


Fig. 2. Simulated results of the iTIP approach

Normalized magnetization (M_{SL}) with inversion pulse “off” and “on” (A, D), M_{iTIP} at the label and reference frequencies in the logarithmic scale (B, E), and asymmetrical spin-locking ratios, SLR_{asym} and $SLR_{iTIP, asym}$ (C, F) were simulated as a function of TSL. A small irradiation pulse power and a small R_2 value lead to high steady state signals (left column), and a high pulse power and a large R_2 lead to low steady state signals (right column). Other parameters used were $\delta = 1$ ppm (400Hz or 2515 rad·s⁻¹), labile proton concentration $P_S = 0.003$, $R_1 = 0.5$ s⁻¹, $k = 1250$ s⁻¹.

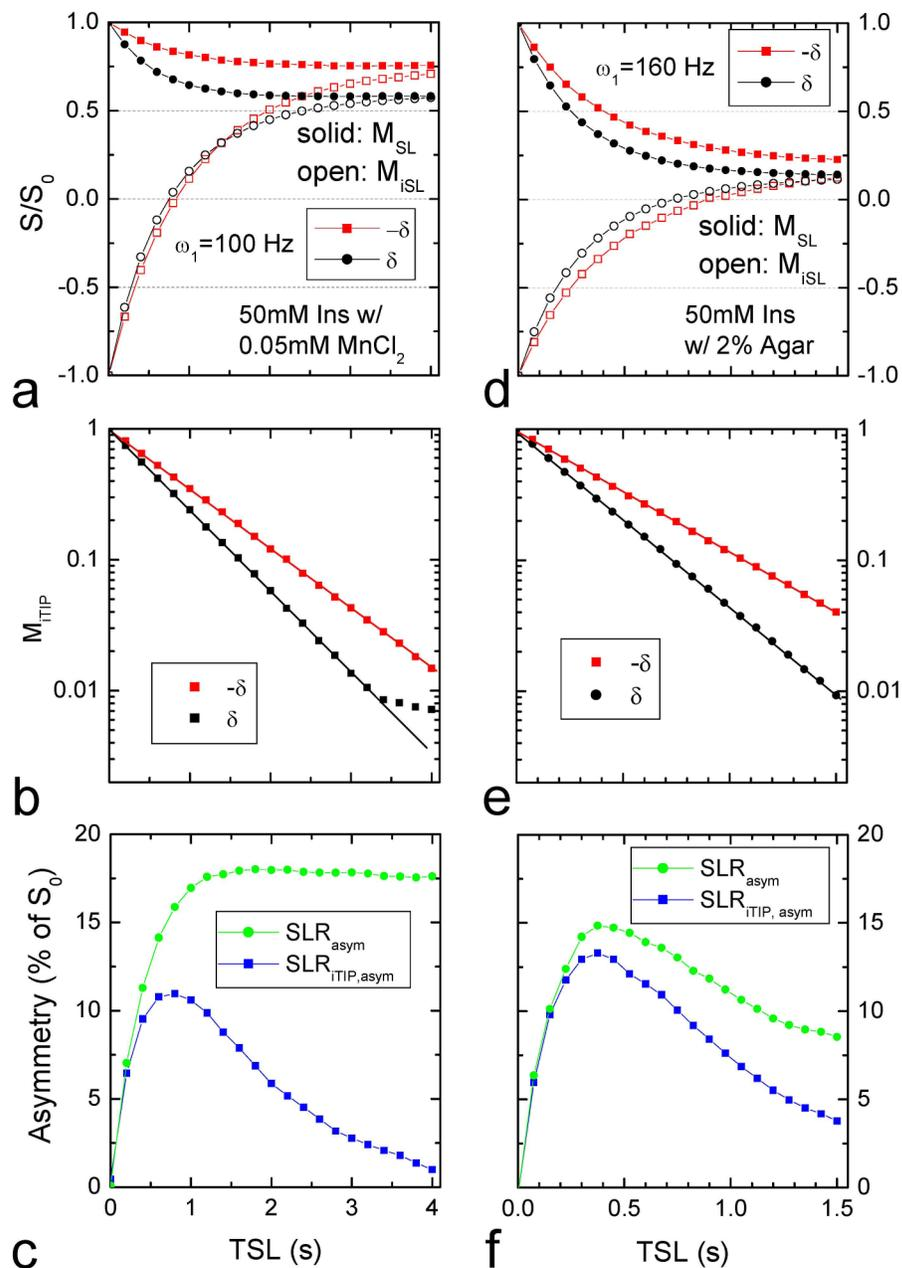


Fig. 3. Experimental iTIP results of 50 mM myo-Inositol with high (A–C) and low steady state conditions (D–F)

The normalized signal was measured with an $\omega_1 = 100$ Hz irradiation pulse for Ins in PBS with 0.05 mM MnCl₂ (left column), and with a 160 Hz pulse for Ins in 2% agar (right column). In both cases, magnetization with inversion “on” and “off” reached the same steady states, and M_{iTIP} decayed monoexponentially with TSL , except for a few data points when the M_{iTIP} becomes very low and dominated by noise (B). Similar to the simulated data in Figure 2, the left column data reached a high steady state and $SLR_{iTIP,asym}$ was significantly smaller than SLR_{asym} for long TSL values (C), while the right column data reached a low steady state, and the peak $SLR_{iTIP,asym}$ was only slightly smaller than the peak SLR_{asym} (F).

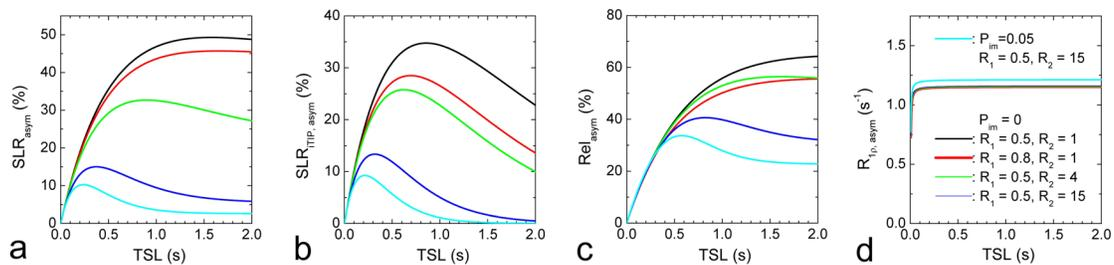


Fig. 4. Independence of $R_{1\rho, \text{asym}}$ on R_1, R_2 and MT effects: simulations

The TSL-dependent SLR_{asym} (A), $SLR_{\text{TIP, asym}}$ (B), Rel_{asym} (C), and $R_{1\rho, \text{asym}}$ (D) were simulated for five R_1, R_2 and P_{im} combinations. Other parameters used were $\delta = 1$ ppm, $P_S = 0.003$, $\omega_1 = 160$ Hz, and $k = 1250 \text{ s}^{-1}$. In (D), all four lines with $P_{\text{im}} = 0$ were overlapping and displayed with different thickness.

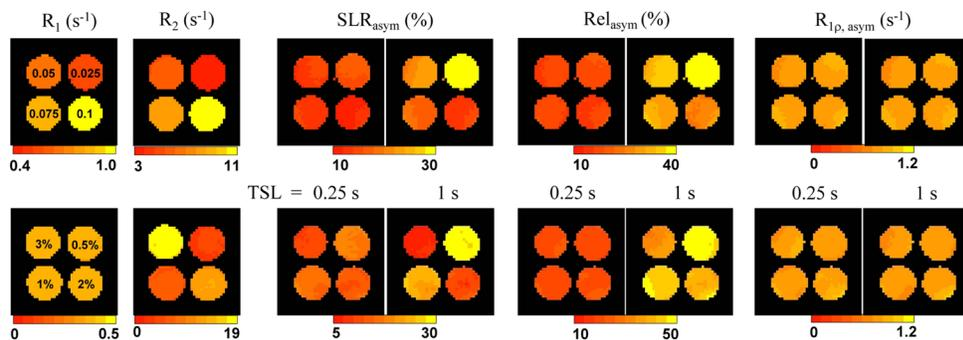


Fig. 5. Independence of $R_{1\rho, \text{asym}}$ on R_1 , R_2 and MT effects: phantom experiments
 For 50mM Ins samples in PBS with MnCl_2 (upper row), both R_1 and R_2 are sensitive to the MnCl_2 concentration (denoted in the R_1 map). For 50 mM Ins in agar mixture (bottom row), only R_2 is sensitive to the agar concentration (denoted in the R_1 map), whereas R_1 is insensitive. SLR_{asym} and Rel_{asym} maps measured with an $\omega_1 = 160$ Hz pulse are almost independent on MnCl_2 and agar concentrations for $TSL = 0.25$ s, but not for a longer TSL of 1.0 s. For all phantoms, the $R_{1\rho, \text{asym}}$ map measured by the iTIP approach appear similar.

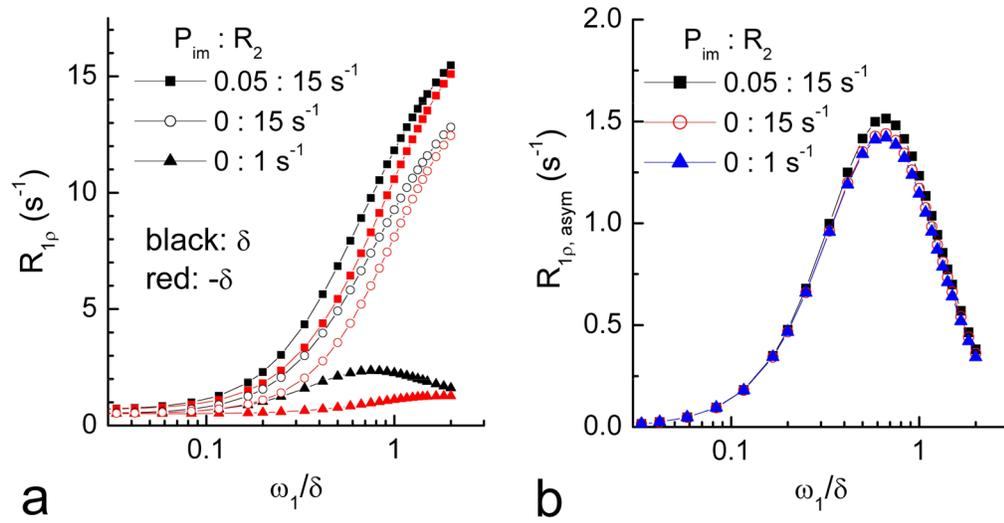


Fig. 6. $R_{1\rho}$ dispersions simulated at the label and the reference frequencies
 $R_{1\rho}$ dispersions are highly dependent on R_2 and P_{im} (A). Such dependence can be removed in the $R_{1\rho,asym}$ dispersion (B).

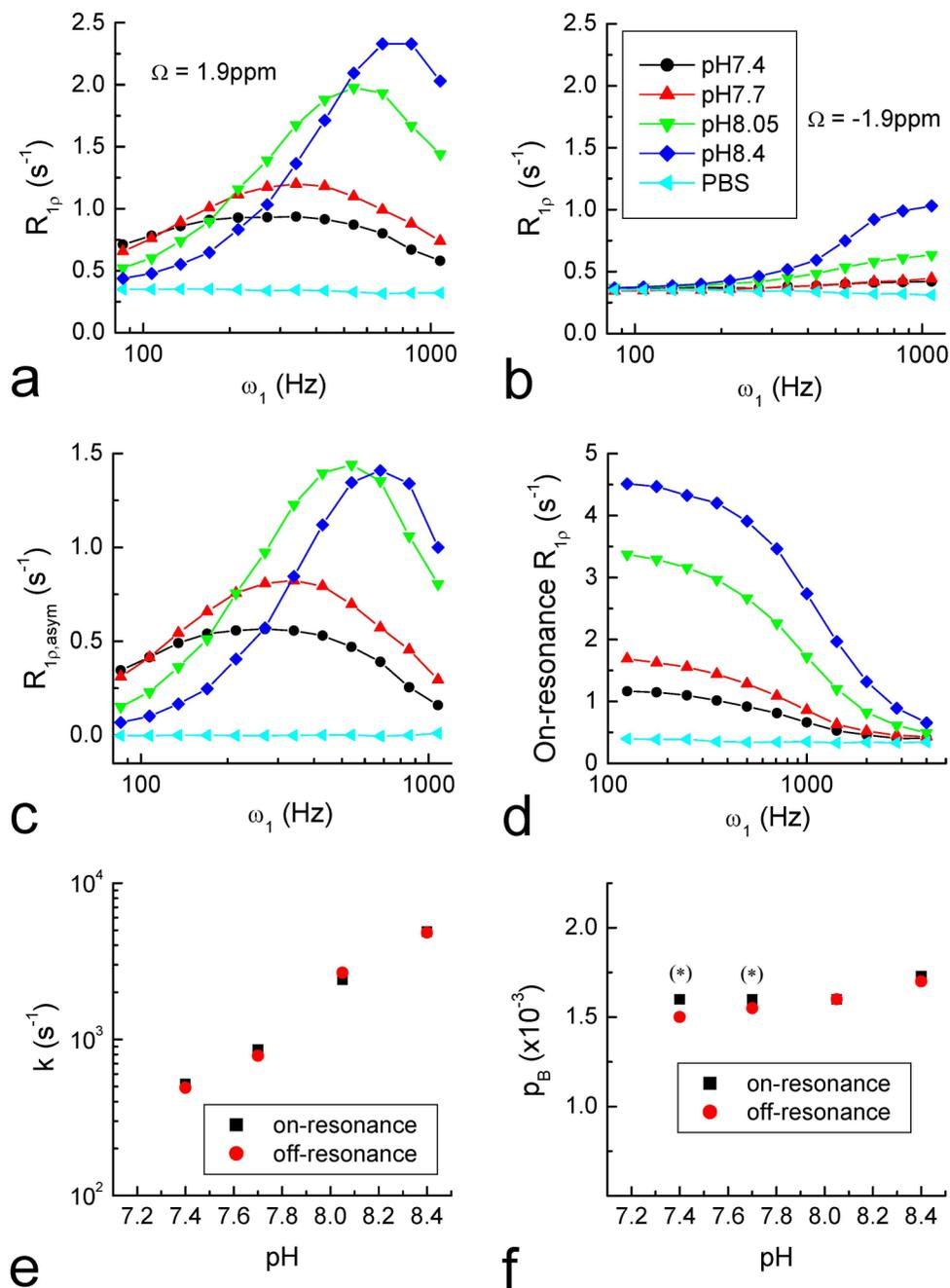


Fig. 7. Off- and on-resonance $R_{1\rho}$ dispersion measurements of Creatine phantoms, and exchange parameter determinations

Off-resonance $R_{1\rho}$ dispersions were measured at 1.9 ppm (A) and -1.9 ppm (B) for PBS only and 50 mM Creatine in PBS with 4 different pH values (indicated in B). The $R_{1\rho,asym}$ dispersion (C) was obtained from the difference of (A) and (B) which removes the R_1 and R_2 effects. The on-resonance $R_{1\rho}$ dispersion increased with pH for these phantoms (D). The fitted results of k (E) and p_B (F) obtained from the dispersions show that $R_{1\rho,asym}$ and on-resonance $R_{1\rho}$ are in reasonable agreement. At low pH values (7.4 and 7.7), k and p_B cannot be determined separately from on-resonance $R_{1\rho}$ dispersion, so their p_B was chosen to be the same as at pH = 8.05 (indicated by asterisks).

Table 1

Parameters used in three-compartment simulation of Bloch-McConnell Equations

Description	Parameter	values
Water pool		
Longitudinal relaxation rate	R_{1w}	0.5 s^{-1} (0.8 s^{-1})
Transverse relaxation rate	R_{2w}	15 s^{-1} (1 s^{-1} , 4 s^{-1})
Relative population	P_w	$1 - P_S - P_{im}$
Labile solute proton		
Longitudinal relaxation rate	R_{1S}	$= R_{1w}$
Transverse relaxation rate	R_{2S}	$= R_{2w}$
Chemical shift from water	δ_S	1 ppm
Relative population	P_S	0.003
Exchange rate with water	k	1250 s^{-1}
Immobile proton		
Longitudinal relaxation rate	$R_{1, im}$	$= R_{1w}$
Transverse relaxation rate	$R_{2, im}$	$10 \mu\text{s}^*$
Chemical shift from water	δ_{im}	0
Relative population	P_{im}	0 (0.05)
Exchange rate with water	k_{im}	50 s^{-1}^*

Several values were varied (shown in parenthesis) to evaluate the effect of those parameters.

* from reference (38).